Smectite fraction assessment in complex natural clay rocks from interlayer water content determined by thermogravimetric and thermoporometry analysis

Denys Grekov, Gilles F Montavon, Jean-Charles Robinet, Bernd Grambow

Smectite fraction assessment in complex natural clay rocks from interlayer water content determined by thermogravimetric and thermoporometry analysis.

Denys Grekov,[a]* Gilles Montavon,[a] Jean-Charles Robinet,[b] Bernd Grambow[a]

[a] IMT Atlantique, SUBATECH, CNRS-IN2P3, Université de Nantes, F-44307 Nantes, France

[b] Andra, R&D Division, Transfer Migration Group, 92298 Châtenay-Malabry, France

Corresponding author: grekov@subatech.in2p3.fr

ABSTRACT

The smectite content is a key parameter to be determined for various applications of clays and clay-rich rocks. The quantity of interlayer water characteristic of swelling domains can be used to assess the smectite content in clays. We propose in this study to use a simple approach to determine water distribution in clays (mainly between pores and interlayers) by means of thermoporometry and thermogravimetric analysis. Provided the interlayer water does not freeze at low temperature upon thermoporometry experiments, the difference between water quantities determined by the two techniques is assigned to interlayer water. Single-phase model clays and complex natural clay rocks and their composites in water-saturated state are characterized by this approach. The open question is the application of available thermoporometry models developed for simple pore geometry to characterize the complex pore network of clays. Depending on the approach used, different pore sizes were obtained highlighting the limit of a simplified model to describe the complex porous network. The results are more coherent when quantifying the amount of interlayer water, further used for smectite content estimation. Good agreement was obtained between smectite fraction contents deduced from the results of thermal analysis and those measured by conventional mineralogical techniques.

KEYWORDS: smectite, interlayer water, pore water, Callovo-Oxfordian clay rock, thermoporometry, thermogravimetric analysis.

INTRODUCTION

Natural clay-rich rock formations or engineered clay-containing materials (compacted clay liner), owing to a combination of their unique properties, such low hydraulic conductivity and high sorption capacity, are considered to be one of the best barriers to prevent the spreading of chemical elements in groundwater in the context of radioactive or industrial waste disposal [1,2]. Illite and smectite phases are frequently the principal constituent of clay-rich rocks. They determine the transport properties of the rock and are known to strongly sorb on their surfaces many radionuclides and toxic chemical species. Often, smectite is found interstratified with illite (I/S) while illite also exists as isolated phase. On contrary to illite, the interlayer space of smectite is accessible for water resulting in structural swelling and interlayer cations exchange. Due to the small size of the clay particles (typically nm to µm) and the large fraction of surface bound water molecules, the mobility of water and solutes is strongly restricted (low hydraulic conductivity and diffusion coefficients) in clay-rich rock.

The characterization of the mineralogical composition of clay-rock and especially of its clay fraction (smectite vs. illite) is of prime importance for the understanding of hydration/swelling properties and sorption/transport processes in these media. To date, crystallographic techniques are considered as reference methods for identification and quantitative analysis of clay phases [3]. The standard protocol consists of X-ray diffraction analysis of < 2 µm clay fraction with several preparations (disordered/orientated, dried/hydrated/glycol-saturated) followed by XRD patterns simulation using Rietveld refinement or related methods, allowing the access to structural and quantitative information [4]. This approach is usually time consuming and require complementary characterizations, including measurements of cationic exchange capacity or elemental analysis. Furthermore, the uncertainty of such approach is in the order of 10-20% depending on mineral complexity [5].

Water uptake in interlayer space (mainly due to hydration of charge-compensating cations) is a specific property of swelling clays differentiating them from other (non-swelling) phyllosilicate phases. Different populations of interlayer water states, usually expressed in terms of 0 up to 3 equivalent monolayers of water molecules, may exist depending on relative humidity, temperature, magnitude of layer charge and its distribution between octahedral and tetrahedral sites, nature of charge-compensating cations or external strengths. Understanding of the hydration properties of swelling clays has been an object of numerous experimental and theoretical studies [6–9]. Several trends can be highlighted: (1) an increase of layer charge shifts the transition 0-to-1 and 1-to-2 water layers to lower relative humidity for both smectite

families featuring the localisation of layer charge in octahedral and tetrahedral sites (montmorillonite and beidellite respectively) [10], (2) under saturation conditions (equilibration at 100 % relative humidity) the amount of interlayer water first increases with the layer charge and then remains nearly-constant or slowly goes down at higher charges when water "competes" with charge-compensating cations for the place in interlayer [11,12], (3) basal spacing, depending on the amount and organisation of interlayer water and cations decreases with layer charge under saturation conditions and in general is larger for smectites with octahedral charge in comparison to smectites with tetrahedral localisation of charge at the same relative humidity [13,14]. Thereby, since interlayer water is characteristic of swelling phases, its content in complex natural argillite samples under controlled humidity conditions is a criterion for quantifying the content of swelling phases - smectities. It should be noticed however that in real complex clay systems, water does not only enter the interlayer space of swelling clays but fills as well the complex pore network formed by arrangement of sheets and other particles in compact media. Analysis of the distribution of water molecules between inter-particle and interlayer states [15] is difficult and appears to be the main challenge of the approach of smectite fraction assessment from interlayer water content.

Interlayer and inter-particle pore water exhibit different physical properties. The non-freezing character of interlayer water, even at very low temperature, is one of its specific characteristics that can be used for the differentiation of water states in clays [16]. ^{1}H low field NMR (spin-spin relaxation time measurement) has emerged as one of methods for the characterization of the distribution of water states in clays [16,17]. The non-freezing character of interlayer water can also be employed for the assessment of water distribution in clay systems by means of thermal analysis. The idea to use thermoporometry for this purpose was introduced by Salles et al. [18]. Originally developed by Brun et al. [19] thermoporometry allows studying the porous structure of solid materials impregnated with liquids. As will be discussed below, the liquid confined in a nano-sized pore will crystallize at lower temperature in comparison to the liquid in "bulk" state, idem for melting processes. The crystallisation/melting temperature of pore-filling water depend on a confinement degree, determined in turn by surface/volume ratio of pores and can be used to access pore sizes and shapes (*vide infra*). In comparison to nitrogen adsorption or mercury intrusion porosimetry (MIP), the thermoporometry is a less commonly employed technique for pore size measurements. However, on contrary to classical techniques requiring sample drying, themoporometry offers the advantage to analyse hydrated (solvated) systems, where the

texture is not damaged by drying processes. It was used for characterization of hydrated organic [20,21] and mineral [22] polymeric gels, mortars [23] and several other classes of materials [24–26].

Salles et al. have first applied thermoporometry for characterization of clays [27]. Simultaneous filling of mesopores (2-50 nm) by capillary water and structural swelling for Na-exchanged montmorillonite was experimentally evidenced for the first time. They illustrated a significant porosity expansion (from 2.25 nm to 4.00 nm) over a large range of hydration degrees upon osmotic swelling of clays. The results of Kozlowski and Walaszczyk for two different montmorillonites suggest however that only the pores larger than 10 nm feature a significant expansion upon relative humidity increase [28], being thus in conflict with the results of Salles et al. Relying on the results of thermoporometry supported by X-ray diffractometry and nitrogen adsorption measurement, Salles et al. determined the ratio between pore and inter-layer water and proposed a mechanism of hydration sequence for a series of powdered montmorillonites with different interlayer cations (Na, Li, Ca, K, Cs) hydrated at different relative humidity (from 11 to 97%) [18].

In water-saturated conditions, the pore network of clay-rich rocks is assumed to be fully filled with water [29]. Upon analysing humidity-equilibrated clays by thermoporometry, the heat released upon specimen cooling, is expected to be due to pore water crystallization, being the only form of water undergoing the liquid-to-solid phase transition in the clay systems. The difference between the total water content (usually determined by means of thermogravimetric analysis) and water content determined by thermoporometry can be attributed to the amount of interlayer water characteristic of swelling phases. This corresponds to the basic assumption of the present study.

Inspired by works of Salles et al. [18,27], we revisited several approaches of thermoporometry in order characterize the distribution of porosity in water-saturated clays and determine the distribution of water forms in these systems. From the quantities of interlayer water, we expect to access the amount of smectite in clay systems of increasing complexity: pure single-phase clays (illite, montmorillonite, interstratified Illite/Smectite), industrial clay-rich material (raw bentonite MX-80) and natural clay-rich rock (the Callovo-Oxfordian mudstone - COx, France).

MATERIALS AND METHODS

Theoretical basis of thermoporometry. Crystallization of a liquid and melting of a solid confined in porous body occur at lower temperature in comparison to the substance in "bulk" state. The shift of phase transition temperature is referred as temperature depression (ΔT). It is inversely proportional to the pore radius, as given by the Gibbs-Thomson equation (1) for cylindrical pore. The measurement of ΔT over a large range of temperatures allows accessing the width of pores filled with the liquid (or crystallized solid).

$$r = \frac{2 \cdot \gamma^{sl} \cdot \vartheta_m \cdot T_0 \cdot cos\theta}{\Delta H_f \cdot \Delta T} \qquad (1)$$

γ^{sl} – interfacial tension on solid/liquid boundary, υ_m – molar volume of pore-filling substance, T_0 – solidification/melting temperature of pore-filling substance in bulk state, ΔT – temperature depression, ΔH_f – change of specific heat of liquid-to-solid phase transition, θ – contact angle.

Technically, thermoporometry is a cryo-Differential Scanning Calorimetry (DSC) experiment, which consists of the measurement of heat flow produced during phase transition of a pore-filling substance, occurring upon progressive cooling and heating of the sample. A hysteresis is usually observed between cooling and heating experiments. According to Brun et al. [19] the hysteresis is related to pore shape and can be quantitatively described by shape factor F, (2).

$$F = \frac{\Delta T_{freezing}}{\Delta T_{melting}} \qquad (2)$$

The originality of thermoporometry as porosity characterization technique consists of the possibility of a direct transformation of the DSC signal into pore size (radius) distribution. By dividing the heat flow measured during the DSC experiment by a temperature-dependant density and a specific heat of phase transition of a substance filling the porous network and by considering the time interval of the measurement, one can determine the volume, of a substance undergoing the crystallization/melting at a given temperature (3).

$$V_{liq(sol)}(T) = \frac{Q(T) \cdot \Delta t}{\Delta H(T)_f \cdot \rho_{liq(sol)}(T)} \qquad (3)$$

where $Q(T)$ – is the heat flow detected during DSC experiment, Δt – the time interval of DSC signal acquisition, and $\rho_{liq(sol)}$ – the density of pore-filling substance. It is recommended to use for data treatment the density of the liquid for cooling cycle and the density of the solid for heating cycle [30].

By considering the pore geometry (factor *m*) and the thickness of a layer of non-freezing substance (in case water δ=0.3…≈1 nm) bounded to pore wall, composed of 1 up to 3 ordered monolayers, as determined by different experimental techniques for water [31–34], one can access a real pore volume filled with the liquid.

$$V_{pore}(T) = V_{liq(sol)}(T) \cdot \left(\frac{r_p(T) + \delta}{r_p(T)}\right)^m \qquad (4)$$

The factor *m* is related to the pore shape. Ideally *m*=3 for spherical pores, *m*=2 for cylindrical pores, *m*=1 for open slit-type pores. The relations between shape factor F and *m* have been discussed by Titulaer et al. [22].

Water is the most commonly used probe liquid for thermoporometry since its interaction with the surfaces is well studied and it features a high specific heat of phase transition, related to the sensitivity of the method, in comparison to organic probes [30]. Whilst the temperature-variation of liquid water (5) and ice (6) densities are well known, the data on water crystallization/melting specific heat temperature-dependence available in the literature is scarce [28].

$$\rho_{liq\ water}(T) = -7.1114 + 0.0882 \cdot T - 3.1959 \cdot 10^{-4} \cdot T^2 + 3.8649 \cdot 10^{-7} \cdot T^3 \qquad (5)$$

$$\rho_{water\ ice}(T) = 0.917 \cdot (1.032 - 1.17 \cdot 10^{-4} \cdot T) \qquad (6)$$

The highest and the lowest boundaries of $\Delta H_f = f(T)$ dispersion [28] can be approximated by the two polynomial formula used in thermoporometry: (7) as introduced by Brun [19] and (8) as introduced by Ishikiryama [35].

$$\Delta H_f^1(T) = 0.0556 \cdot \left(T - T_f^0\right)^2 + 7.43 \cdot \left(T - T_f^0\right) + 332 \qquad (7)$$

$$\Delta H_f^2(T) = 334.1 + 2.119 \cdot \left(T - T_f^0\right) - 0.00783 \cdot \left(T - T_f^0\right)^2 \qquad (8)$$

where T_f° is the equilibrium fusion temperature of ice.

Many authors prefer a direct transformation of DSC signal to dV_p/dr_p scale, being useful for visual comparative analysis of fine porosity variations within a series of samples. In the present work, we mainly exploit the cumulative curves, providing more realistic, quantitative, information on pore size distribution (PSD), in order to determine the pore volumes of humidity-equilibrated clays filled with capillary-condensed water.

The transformation of a temperature axis of a DSC curve into pore width scale is also a straightforward procedure requiring the introduction of assumptions related to the pore shape

and thickness of a layer of non-freezing water. By factoring the experimentally-determined temperature dependence of different physical properties of water in equation (1), Brun et al. [19] proposed simplified expressions relying the depression of crystallization/melting temperature to the radius of cylindrical pores, (9). To the best of our knowledge, no analytical expression is available for ΔT transformation to pore width for slit-type pore geometry, characteristic of layered systems. The empirical formulas, obtained from calibration curves, rely strongly on thermoporometry measurements for a series of model materials with well-known pore sizes, available as well for the transformation of temperature depression data to pore sizes. Most of the empirical approaches were developed for the description of cylindrical pores of different sizes [20,30,34,35]. The formulas of Landry (10) deserve a special attention since in his approach the material with irregular pore shapes (mesoporous glass with r_p ranging between 3.5 and 100 nm) was used for establishing calibration curves [30].

$$r_p(melting) = \frac{19.082}{\Delta T + 0.1207} + 1.15 \qquad r_P(freezing) = -\frac{38.558}{\Delta T - 0.1719} + 0.04 \qquad (9)$$

$$r_p(melting) = -\frac{32.33}{\Delta T} + 0.68 \qquad r_P(freezing) = -\frac{64.67}{\Delta T} + 0.57 \qquad (10)$$

One should notice that water films composed of several molecular layers on the external surfaces of clay particles or adsorbed on the walls of mesopores (non-filed with capillary condensate), may feature high confinement degree or even the non-freezing character and contribute to narrow pores or interlayer water respectively [19]. Thereby, in order to minimize this effect, a complete saturation of samples with water is mandatory.

Thermoporometry procedure. 20-40 mg of humidity-saturated clay samples (equilibrated in a desiccator containing liquid water), in 40 µL closed aluminum crucibles were analysed with a DSC 1 Mettler Toledo calorimeter. The experimental procedure includes 4 cycles: (1) rapid cooling of the sample from ambient temperature down to -60 °C (at -5 °/min) in order to freeze all pore water, (2) heating from -60 up to -0.5 °C (at 1 °/min) in order to ensure a non-complete melting of ice crystals, (3) cooling down to -60 °C (at 1 °/min), (4) heating up to the ambient temperature (at 1 °/min) in order to achieve a complete melting of ice. Heat flow from the sample is measured upon temperature variation. A 20 ml/min flow of nitrogen gas was used for homogeneous heat transfer.

Materials and sample preparation. Bentonite Kunipia F was received from Kunimine industries. After dispersion in deionized water (5 g/l) the <2 µm fraction was extracted by centrifugation at 1000 rpm. Na- and Ca- exchanged forms (pure-phase montmorillonites,

Mmt) were obtained by following the standard protocol including 24 h contact with 0.2 mol/l NaCl or $CaCl_2$ solution respectively, 5 cycles of centrifugation at 20000 rpm and washing in deionized water, final washing in methanol and drying of suspension at 50 °C. As given by various authors this type of montmorillonite features layer charge ranging between -0.7 and -0.8 per unit cell, mainly localized in octahedral positions of phyllosilicate sheets [36,37]. Interstratified Illite-Smectite ISCz-1 (I/S ratio ≈ 70/30) was received from Clay Minerals Society, the clay fraction was extracted by elutriation procedure [38] and further transformed in Na-exchanged form in the same way as montmorillonite samples. According to bibliographic data this phase is characterized by an average charge of ≈-1.3 per unit cell, distributed between octahedral and tetrahedral positions of phyllosilicate sheets of illite and smectite domains [39]. A similar procedure was applied for Illite du Puy [40] and clay fraction of natural clay-rock (Callovo-Oxfordian mudstones) purification. Illite du Puy features layer charge close to -1.7 per unit cell, distributed, similarly to ISCz-1 between octahedral and tetrahedral positions [41]. Clay-rich industrial material bentonite MX-80 was directly Na-exchanged without further purification. It features similar structural characteristics as montmorillonite of Kunimine industries [42]. The core samples of natural clay-rock come from the Callovo-Oxfordian (COx) mudstones (East of Paris basin, France). Callovo-Oxfordian clay rock is mainly composed of clay minerals (mainly illite and interlayered I/S phases), carbonates (C) and tectosilicates (T) [43]. Pores in the Callovo-Oxfordian mudstone are typically lower than 1 µm and mostly distributed in its clay fraction (inter-particle and inter-sheet) while the contribution of other minerals, for instance carbonates and tectosilicates, to clay rock porosity is minor [44,45]. Several depths were selected in order to analyse the clay rocks with various clay fractions and I/S ratios. The simplified mineralogical characteristics of the samples are summarized in Table 1S. It has been illustrated that cation exchange properties of clay fraction of COx argillite (related to layer charge and illite/smectite ratio) can be described in a “bottom-up” approach [46] relying on retention properties of pure illite and montmorillonite as considered in the present work.

All samples were grinded manually and sieved to collect the size fraction <100 µm. Powdered samples were equilibrated at ≈100 % relative humidity at 20 °C inside a desiccator containing liquid water during 1 month. It should be noticed that in case of Callovo-Oxfordian mudstone, particles size fraction < 100 µm is representative of clay rock microstructure [47].

Thermo-gravimetric analysis (TGA). The measurements of total water content were carried out with Setaram TG-DSC 111 thermo-gravimetric analyzer. 5-20 mg of hydrated clays were heated in quartz crucibles from ambient temperature up to 715 °C under 20 ml/l of He flow. Temperature-induced masse variations were corrected by subtracting the TGA curves acquired for an empty crucible.

RESULTS AND DISCUSSIONS

Pore size measurement. A cryo-DSC curve of humidity-saturated Na-bentonite is represented in Figure 1 a). A sharp peak on the first curve of rapid cooling is due to a spontaneous crystallization of overcooled water in porous network. An incomplete melting of ice upon the first heating cycle allows preserving a small fraction of ice crystals, playing the role of crystallization germs upon the second cooling cycle, preventing overcooling. Several procedures of DSC baseline processing have been proposed in the literature [48]. Given the DSC signal obtained for an empty crucible is almost flat, we adapted a linear baseline correction in the present work, to obtain the same total heat of crystallization and melting upon cooling and heating of hydrated samples.

The approaches of Brun and Landry discussed earlier were applied for DSC signal (second cooling and second heating cycles) transformation into pore size distribution. The results for Na-montmorillonite are compared in Figure 1 b) and c) for cooling and heating cycles respectively. It should be noticed that both models have been developed for average-size (3…50 nm) mesopores analysis, detectable between 0 and approximately -20 °C (Landry) or -40 °C (Brun) upon DSC measurements. In narrow mesopores however, water is strongly confined and the contribution of a layer of non-freezing water to pore volume is significant. Several clay systems studied in the present work feature the DSC signals below -30 °C, originating most probably from small-size mesopores. Jahnert et al. [34] analysed by thermoporometry a series of MCM-type materials with r_p ranging between 2.25 and 1.5 nm, giving the DSC signals between -33 and -60 °C respectively. For these systems with well-defined pore sizes, the measured freezing temperature depressions were in a good agreement with those predicted by the extended model of Brun for corresponding pore sizes. Thus, in order to account for low-temperature contributions for several systems studied herein, relying on the observations of Jahnert et al. and on the linearity of the model of Landry, we extended the above mentioned models to lower temperatures, supposing that water behaviour is the

same over the whole range of temperature variation. The details on pore volume calculation are discussed below.

A good agreement is observed between the values of maxima on PSD curves obtained from cooling and heating experiments. For all samples analysed in the present work there is a shift in the curves of pore radius distribution comparing the methods of Landry and Brun. This trend had already been reported by Landry in his original work. Most probably, the divergence is related to the pore shape considered by the model, since this characteristic determines the curvature of solid/liquid interface, being in turn one of factors influencing the temperature depression within a given pore size.

The sizes of pores determined from cooling and heating experiments via the methodologies of Brun and Landry for humidity-saturated clays are summarised in Table 1, the full data is available in Figure 1S. Most of the Callovo-Oxfordian clay rock samples show the narrower pores in comparison to model clay systems (<10 nm), which is due to their higher degree of compaction acquired during diagenesis. The same order of magnitude of pore sizes for Callovo-Oxfordian clay rock sample was evidenced relying on 3D FIB-SEM image reconstruction [40,45] or conventional MIP and N_2 adsorption [44]. Without controlled mechanical stress conditions, it is difficult however to compare the pore sizes determined by thermoporometry for humidity-saturated clays with those accessed by conventional techniques (usually dehydrated samples are analysed) since this characteristic is significantly influenced by structural and osmotic swelling. Numerous bibliographic studies have validated thermoporometry as porosity characterization technique, nevertheless one should keep in mind that the results are model-dependant and their accuracy depends on the closeness of the chosen model to a real system.

Pore volume measurement and water distribution analysis. The maxima on cumulative curves of PSD determine the pore volumes occupied by capillary-condensed water in humidity-saturated clays. As introduced earlier, several assumptions are needed to access this characteristic from PSD: pore geometry, thickness of a layer of non-freezing water being close to the pore wall and the variation of ΔH_f with the temperature. We calculated cumulative pore volumes according to the models of Brun and Landry by considering the average value of thickness of a layer of non-freezing water (δ=0.6 nm as frequently used in the literature), but also its extreme values (i.e. 0.3 and 0.9 nm). It is recommended to exploit the hysteresis between freezing and melting curves in order to determine the pore shape factor needed for pore volume calculation [19]. In case of complex systems with significant pore

size distributions and a complex pore shape (leading to broad DSC signals) it is difficult to define discrete sets of freezing and melting signals for each domain of pore sizes. Thus, we assumed a cylindrical pore shape (m=2) for the model of Brun as given in the original literature [19] and both, cylindrical (m=2) and slit-type (m=1) geometries for the model of Landry. The volumes of pores filled with water were deduced from an average between cooling and heating cycles, as recommended in the literature, as well as from the results of individual sequences of cooling and heating. Both the expressions (7) and (8) were considered to account for ΔH_f variation with the temperature. Yellow bars on the histograms in Figures 3S-5S (see supplementary information) depict the pore volumes determined from thermoporometry. The corresponding error bars are related to the thickness of a layer of non-freezing water bounded to pore wall.

The total water content in humidity-equilibrated clays was determined by thermogravimetric analysis. Many works have illustrated that almost complete drying of clays occurs below 200 °C, whereas pronounced dehydroxylation usually starts at temperatures higher than 400 °C [49]. The TGA thermograms for single-phase and multicomponent clay systems are represented in Figure 2S. Since for all samples only very little mass variation is detected between 200 and 400 °C, we attributed the weight loss at 200 °C to the total water content.

From the total water content determined by TGA and pore water (composed of freezing and non-freezing forms) content determined by thermoporometry, one can access the amount of interlayer water, supposing that pore and interlayer water are principal forms of water characteristic of humidity-saturated clays. Water distribution for clay samples determined by using the model of Brun in combination with the expression (7), as an average between cooling and heating cycles are represented in Figure 2. Water distributions have been determined for all clay samples considering the entire range of clauses mentioned in previous paragraphs (difference of results of cooling and heating cycles, two thermoporometry models, two geometrical factors, two expressions for ΔH_f variation with the temperature, uncertainty of the thickness of a layer of non-freezing water); the results are graphically represented in Figures 3S-5S.

The models of Brun and Landry considering slit geometry give close water distributions. The uncertainties related to the thickness of a layer of non-freezing pore water are also close. When the model of Landry considering cylindrical pore geometry is used, the determined fractions of interlayer water are lower and the associated uncertainties are larger in comparison to two former models. Regardless the geometrical considerations, the fraction of

interlayer water in water distribution is systematically higher when the expression (8) is used to account for ΔH_f variation with the temperature.

In order to choose the approach giving the most accurate water distribution, we will compare the quantities of interlayer water in pure clay phases with those from the literature: Na-exchanged montmorillonite and illite. Ferrage et al. [12] analysed by crystallographic methods two synthetic Na-exchanged smectites (layer charge 0.8 and 1.4) equilibrated with water at relative humidity ranging between 0 and 92%. They illustrated that regardless the difference in layer charge, at relative humidity close to saturation, both smectites contain about 0.21 g of interlayer water per g of dry clay. According to molecular modelling prediction [11], smectites under saturation conditions feature ≈ 0.12-0.26 g water/g dry clay, depending on the magnitude and localization of layer charge. The smectites with layer charge close to 0.8 (present work and [12]), contain ≈ 0.2 g water/g dry clay, in an excellent agreement with experimental data. On the other hand, the non-swelling pure-phase illites, do not contain interlayer water [50], its small fraction however, if detected, is related to the contamination by 2-5% of smectite being difficult to separate [40]. Thereby, the models of Brun considering cylindrical pore geometry and Landry considering slit-type pore geometry in combination with expression (7) and the model of Landry considering cylindrical pore geometry in combination with expression (8) allow for interlayer water content to be >0.21 g/g of dry clay and close to 0 g/g of dry clay for Na-exchanged montmorillonite and illite respectively. This validates the mentioned models for water distribution analysis.

Smectite fraction assessment. Admitting that interlayer and pore water are two principal states of water in humidity-saturated clays and that smectite fraction of COx argillite feature close characteristics (layer charge and consequently interlayer water and cations content) as pure-phase montmorillonite isolated from industrial bentonite [43,46], we can access smectite fraction in different clay systems from interlayer water content. Pure Na-montmorillonite was chosen as reference for Na-exchanged clays. For natural clay-rich rocks Ca^{2+} and Na^{+} are principle cations in swelling and exchangeable domains [51]. Without having analysed the exact content of these species we consider a ratio 1:1, as given in the literature, so an average interlayer water content between Ca^{2+} and Na^{+} exchanged montmorillonites was used as a reference for smectite fraction estimation in natural clays. The smectite fractions measured by thermoporometry (by following different approaches discussed in previous paragraphs) are compared with those determined by conventional methods in Figure 3. The vertical error bars, being the most important uncertainty are related to the difference between the results of

cooling and heating cycles. In most cases the uncertainties related to a thickness of a layer of non-freezing water are narrower than error bar.

In order to quantitatively compare the results obtained from different models we calculated the residual sum of squares (RSS) – Σ for experimental points. The approaches giving water distribution being in a good agreement with the bibliographic data for model systems (i.e. model of Brun considering cylindrical pore geometry in combination with expression (7), model of Landry considering slit-type pore geometry in combination with expression (7) and model of Landry considering cylindrical pore geometry in combination with expression (8)) allow for the lowest RSS when smectite fraction is calculated.

CONCLUSION

Thermoporometry was used for pore size and pore volume measurements for a series of humidity-saturated powdered model mono-phase clays, raw bentonite MX-80, complex natural clay-rock samples (the Callovo-Oxfordian formation) and argillite clay fraction. We employed the models proposed in works of Brun and Landry for pore size determining from crystallization/melting temperatures of water/ice confined in porous body. Pore sizes determined by thermorometry for natural argillite samples are in a good agreement with bibliographic data. When calculating the pore volumes, we accounted for the uncertainty of water crystallization specific enthalpy variation with the temperature and for that of the thickness of a layer of non-freezing water, available in the literature. By supposing that pore and interlayer water are major water forms in humidity-saturated clays, we determined water distribution for a series of clay samples of different complexity relying on the results of thermoporometry and thermogravimetric analysis. A good agreement between interlayer water content determined by thermal analysis with that available in the literature (experimental and molecular modelling data) for pure-phase model clays, allowed us to validate several approaches of thermoporometry for water distribution analysis in clays: model of Brun considering cylindrical pores in combination with expression (7), model of Landry considering slit-type pores in combination with expression (7) and model of Landry considering cylindrical pores in combination with expression (8). Any of these models can be chosen without increasing the uncertainty in determining the water distribution in clays. The interlayer water in clay minerals has been proposed as diagnostic criterion for smectite (swelling) fraction content assessment. From the quantities of interlayer water we calculated smectite fraction content by considering purified montmorillonite as reference system.

Smectite contents determined from interlayer water amount and by mineralogical analysis are compared. The approaches of thermoporometry, validated on model clays for water forms distribution analysis, allow the determination of the smectite fraction of complex clay rock to be in a good agreement with that measured by mineralogical analysis.

As illustrated in the present work, a combined approach of thermogravimetric analysis and thermoporometry appears to be a direct and simple method for water distribution analysis in powdered clay systems. The method we propose can be employed for water distribution analysis in intact clay rock. In this context, the influence on water distribution of mechanical constrains, of temperature and layer charge of the smectite fraction are key elements to be understood.

Acknowledgements

The present work was supported by the industrial chair "Storage and Disposal of Radioactive Waste" at the Institut Mines-Télécom Atlantique, funded by ANDRA, Orano, and EDF. We thank Dr. Rodica Chiriac from "Laboratoire des Multimatériaux et Interfaces" - UMR 5615 (Université de Lyon) for thermoporometry measurements and Dr. Solange Ribet (Subatech) for advices for data treatment.

References

[1] B. Grambow, Geological disposal of radioactive waste in Clay, Elements. 12 (2016) 239–245. doi:10.2113/gselements.12.4.239.

[2] B. Wang, J. Xu, B. Chen, X. Dong, T. Dou, Hydraulic conductivity of geosynthetic clay liners to inorganic waste leachate, Appl. Clay Sci. 168 (2019) 244–248. doi:10.1016/j.clay.2018.11.021.

[3] D. M. Moore, R. C. Reynolds, X-Ray Diffraction and the Identification and Analysis of Clay Minerals. Oxford University Press, Oxford., 1997.

[4] D.L. Bish Studies of clays and clay minerals using X-ray powder diffraction and the Rietveld method, Chapter 4, R.C. Reynolds Jr., J.R. Walker (Eds.), Computer Applications to X-ray Powder Diffraction Analysis of Clay Minerals, CMS Workshop Lectures, 1993.

[5] D.A. McManus, Suggestions for authors whose manuscripts include quantitative clay mineral analysis by X-ray diffraction, Mar. Geol. 98 (1991) 1–5. doi:10.1016/0025-

444 3227(91)90030-8.

445 [6] R. Torrence Martin, Adsorbed Water on Clay: A Review, Clays Clay Miner. 9 (1960)
446 28–70. doi:10.1346/CCMN.1960.0090104.

447 [7] R.T. Cygan, J.A. Greathouse, H. Heinz, A.G. Kalinichev, Molecular models and
448 simulations of layered materials, J. Mater. Chem. 19 (2009) 2470–2481.
449 doi:10.1039/b819076c.

450 [8] C.D. Hatch, J.S. Wiese, C.C. Crane, K.J. Harris, H.G. Kloss, J. Baltrusaitis, Water
451 adsorption on clay minerals as a function of relative humidity: Application of BET and
452 Freundlich adsorption models, Langmuir. 28 (2012) 1790–1803.
453 doi:10.1021/la2042873.

454 [9] E. Ferrage, Investigation of the interlayer organization of water and ions in smectite
455 from the combined use of diffraction experiments and molecular simulations. A review
456 of methodology, applications, and perspectives, Clays Clay Miner. 64 (2016) 348–373.
457 doi:10.1346/CCMN.2016.0640401.

458 [10] E. Ferrage, B. Lnson, B. Sakharov, N. Geoffroy, E. Jacquot, V. Drits, Investigation of
459 dioctahedral smectite hydration properties by modeling of X-ray diffraction pro fi les :
460 In fl uence of layer charge and charge location, Am. Mineral. 92 (2007) 1731–1743.
461 doi:10.2138/am.2007.2273.

462 [11] K. Emmerich, N. Giraudo, R. Schuhmann, F. Schnetzer, H. Kaden, P. Thissen, On the
463 Prediction of Water Contents in Na-Saturated Dioctahedral Smectites, J. Phys. Chem.
464 C. 122 (2018) 7484–7493. doi:10.1021/acs.jpcc.7b11953.

465 [12] E. Ferrage, B. Lanson, L.J. Michot, J.L. Robert, Hydration properties and interlayer
466 organization of water and ions in synthetic na-smectite with tetrahedral layer charge.
467 Part 1. Results from X-ray diffraction profile modeling, J. Phys. Chem. C. 114 (2010)
468 4515–4526. doi:10.1021/jp909860p.

469 [13] B. Dazas, B. Lanson, A. Delville, J.L. Robert, S. Komarneni, L.J. Michot, E. Ferrage,
470 Influence of tetrahedral layer charge on the organization of interlayer water and ions in
471 synthetic Na-saturated smectites, J. Phys. Chem. C. 119 (2015) 4158–4172.
472 doi:10.1021/jp5123322.

473 [14] D.A. Laird, Influence of layer charge on swelling of smectites, Appl. Clay Sci. 34
474 (2006) 74–87. doi:10.1016/j.clay.2006.01.009.

475 [15] C. Tournassat, C.A.J. Appelo, Modelling approaches for anion-exclusion in compacted
476 Na-bentonite, Geochim. Cosmochim. Acta. 75 (2011) 3698–3710.
477 doi:10.1016/j.gca.2011.04.001.

478 [16] G. Montavon, Z. Guo, C. Tournassat, B. Grambow, D. Le Botlan, Porosities accessible
479 to HTO and iodide on water-saturated compacted clay materials and relation with the
480 forms of water: A low field proton NMR study, Geochim. Cosmochim. Acta. 73 (2009)
481 7290–7302. doi:10.1016/j.gca.2009.09.014.

482 [17] M. Fleury, E. Kohler, F. Norrant, S. Gautier, J. M'Hamdi, L. Barré, Characterization
483 and quantification of water in smectites with low-field NMR, J. Phys. Chem. C. 117
484 (2013) 4551–4560. doi:10.1021/jp311006q.

485 [18] F. Salles, O. Bildstein, J.M. Douillard, M. Jullien, J. Raynal, H. Van Damme, On the
486 cation dependence of interlamellar and interparticular water and swelling in smectite
487 clays, Langmuir. 26 (2010) 5028–5037. doi:10.1021/la1002868.

488 [19] M. Brun, A. Lallemand, J.F. Quinson, C. Eyraud, A new method for the simultaneous
489 determination of the size and shape of pores: the thermoporometry, Thermochim. Acta.
490 21 (1977) 59–88. doi:10.1016/0040-6031(77)85122-8.

491 [20] M. Iza, S. Woerly, C. Danumah, S. Kaliaguine, M. Bousmina, Determination of pore
492 size distribution for mesoporous materials and polymeric gels by means of DSC
493 measurements: Thermoporometry, Polymer (Guildf). 41 (2000) 5885–5893.
494 doi:10.1016/S0032-3861(99)00776-4.

495 [21] M. Baba, J.M. Nedelec, J. Lacoste, J.L. Gardette, Calibration of cyclohexane solid-
496 solid phase transition thermoporosimetry and application to the study of crosslinking of
497 elastomers upon aging, J. Non. Cryst. Solids. 315 (2003) 228–238. doi:10.1016/S0022-
498 3093(02)01610-1.

499 [22] M.K. Titulaer, J.C. van Miltenburg, J.B.H. Jansen, J.W. Geus, Thermoporometry
500 applied to hydrothermally aged silica hydrogels, Recl. Des Trav. Chim. Des Pays-Bas.
501 114 (1995) 361–370. doi:10.1002/recl.19951140804.

502 [23] Z. Sun, G.W. Scherer, Pore size and shape in mortar by thermoporometry, Cem. Concr.
503 Res. 40 (2010) 740–751. doi:10.1016/j.cemconres.2009.11.011.

504 [24] K.R. Kloetstra, H.W. Zandbergen, M.A. van Koten, H. van Bekkum, Thermoporometry
505 as a new tool in analyzing mesoporous MCM-41 materials, Catal. Letters. 33 (1995)

145–156. doi:10.1007/BF00817054.

[25] F. Chassagneux, R. Chiriac, F. Bessueille, M. Karabulut, L. Bois, S. Parola, Ellipsoporosimetry and thermoporometry analyses of mesoporous titania film containing silver nanoparticles, Microporous Mesoporous Mater. 139 (2011) 52–58. doi:10.1016/j.micromeso.2010.10.016.

[26] D. Majda, W. Makowski, M. Mańko, Pore size distribution of micelle-templated silicas studied by thermoporosimetry using water and n-heptane, J. Therm. Anal. Calorim. 109 (2012) 663–669. doi:10.1007/s10973-012-2372-9.

[27] F. Salles, I. Beurroies, O. Bildstein, M. Jullien, J. Raynal, R. Denoyel, H. Van Damme, A calorimetric study of mesoscopic swelling and hydration sequence in solid Na-montmorillonite, Appl. Clay Sci. 39 (2008) 186–201. doi:10.1016/j.clay.2007.06.001.

[28] T. Kozlowski, Ł. Walaszczyk, Analyzing expanding clays by thermoporometry using a stochastic deconvolution of the DSC signal, Clays Clay Miner. 62 (2014) 386–402. doi:10.1346/CCMN.2014.0620503.

[29] C.A.J. Appelo, P. Wersin, Multicomponent diffusion modeling in clay systems with application to the diffusion of tritium, iodide, and sodium in opalinus clay, Environ. Sci. Technol. 41 (2007) 5002–5007. doi:10.1021/es0629256.

[30] M.R. Landry, Thermoporometry by differential scanning calorimetry: Experimental considerations and applications, Thermochim. Acta. 433 (2005) 27–50. doi:10.1016/j.tca.2005.02.015.

[31] T. Sakamoto, H. Nakamura, H. Uedaira, A. Wada, High-frequency dielectric relaxation of water bound to hydrophilic silica gels, J. Phys. Chem. 93 (1989) 357–366. doi:10.1021/j100338a069.

[32] M. Tasaka, S. Suzuki, Y. Ogawa, M. Kamaya, Freezing and nonfreezing water in charged membranes, J. Memb. Sci. 38 (1988) 175–183. doi:10.1016/S0376-7388(00)80878-9.

[33] P.J. Davis, C. Jeffrey Brinker, D.M. Smith, Pore structure evolution in silica gel during aging/drying I. Temporal and thermal aging, J. Non. Cryst. Solids. 142 (1992) 189–196. doi:10.1016/S0022-3093(05)80025-0.

[34] S. Jähnert, F. Vaca Chávez, G.E. Schaumann, A. Schreiber, M. Schönhoff, G.H. Findenegg, Melting and freezing of water in cylindrical silica nanopores, Phys. Chem.

537 Chem. Phys. 10 (2008) 6039–6051. doi:10.1039/b809438c.

538 [35] K.M. Ishikiriyama, M. Todoki, Pore Size Distribution (PSD) Measurements of Silica
539 Gels by Means of Differential Scanning Calorimetry: I. Optimization for Determination
540 of PSD, J. Colloid Interface Sci. 171 (1995) 92–102. doi:10.1006/jcis.1995.1154.

541 [36] T. Okada, Y. Ehara, M. Ogawa, Adsorption of Eu3+ to smectites and fluoro-tetrasilicic
542 mica, Clays Clay Miner. 55 (2007) 348–353. doi:10.1346/CCMN.2007.0550402.

543 [37] K. Idemitsu, H. Kozaki, M. Yuhara, T. Arima, Y. Inagaki, Diffusion behavior of
544 selenite in purified bentonite, Prog. Nucl. Energy. 92 (2016) 279–285.
545 doi:10.1016/j.pnucene.2015.08.012.

546 [38] C. Tournassat, H. Gailhanou, C. Crouzet, G. Braibant, A. Gautier, A. Lassin, P. Blanc,
547 E.C. Gaucher, Two cation exchange models for direct and inverse modelling of
548 solution major cation composition in equilibrium with illite surfaces, Geochim.
549 Cosmochim. Acta. 71 (2007) 1098–1114. doi:10.1016/j.gca.2006.11.018.

550 [39] K. Ufer, R. Kleeberg, J. Bergmann, R. Dohrmann, Rietveld refinement of disordered
551 illite-smectite mixed-layer structures by a recursive algorithm. I: One-dimensional
552 patterns, Clays Clay Miner. 60 (2012) 507–534. doi:10.1346/CCMN.2012.0600507.

553 [40] S. Gaboreau, J.C. Robinet, D. Prêt, Optimization of pore-network characterization of a
554 compacted clay material by TEM and FIB/SEM imaging, Microporous Mesoporous
555 Mater. 224 (2016) 116–128. doi:10.1016/j.micromeso.2015.11.035.

556 [41] C. Poinssot, B. Baeyens, M.H. Bradbury, Experimental and modelling studies of
557 caesium sorption on illite, Geochim. Cosmochim. Acta. 63 (1999) 3217–3227.
558 doi:10.1016/S0016-7037(99)00246-X.

559 [42] B. Jönsson, T. Åkesson, B. Jönsson, S. Meehdi, J. Janiak, R. Wallenberg, Structure and
560 forces in bentonite MX-80, Tech. Rep. TR-09-06 (2009).

561 [43] E. Gaucher, C. Robelin, J.M. Matray, G. Négrel, Y. Gros, J.F. Heitz, A. Vinsot, H.
562 Rebours, A. Cassagnabère, A. Bouchet, ANDRA underground research laboratory:
563 Interpretation of the mineralogical and geochemical data acquired in the Callovian-
564 Oxfordian formation by investigative drilling, Phys. Chem. Earth. 29 (2004) 55–77.
565 doi:10.1016/j.pce.2003.11.006.

566 [44] B. Yven, S. Sammartino, Mineralogy, texture and porosity of Callovo-Oxfordian
567 argillites of the Meuse/Haute-Marne region (eastern Paris Basin), Mémoires La Société

568 Géologique Fr. 178 (2007) 73–90.

569 [45] Y. Song, C.A. Davy, D. Troadec, A.M. Blanchenet, F. Skoczylas, J. Talandier, J.C.
570 Robinet, Multi-scale pore structure of COx claystone: Towards the prediction of fluid
571 transport, Mar. Pet. Geol. 65 (2015) 63–82. doi:10.1016/j.marpetgeo.2015.04.004.

572 [46] C. Tournassat, H. Gailhanou, C. Crouzet, G. Braibant, A. Gautier, E.C. Gaucher,
573 Cation Exchange Selectivity Coefficient Values on Smectite and Mixed-Layer
574 Illite/Smectite Minerals, Soil Sci. Soc. Am. J. 73 (2009) 928.
575 doi:10.2136/sssaj2008.0285.

576 [47] J.C. Robinet, P. Sardini, D. Coelho, J.C. Parneix, D. Prt, S. Sammartino, E. Boller, S.
577 Altmann, Effects of mineral distribution at mesoscopic scale on solute diffusion in a
578 clay-rich rock: Example of the Callovo-Oxfordian mudstone (Bure, France), Water
579 Resour. Res. 48 (2012) 1–17. doi:10.1029/2011WR011352.

580 [48] K. Singh, Modeling Differential Scanning Calorimetry, Thermochim. Acta. 159 (1990)
581 267–298.

582 [49] L. Tajeddine, H. Gailhanou, P. Blanc, A. Lassin, S. Gaboreau, P. Vieillard, Hydration-
583 dehydration behavior and thermodynamics of MX-80 montmorillonite studied using
584 thermal analysis, Thermochim. Acta. 604 (2015) 83–93. doi:10.1016/j.tca.2015.02.002.

585 [50] S. Nir, Y. El Nahhal, T. Undabeytia, G. Rytwo, T. Polubesova, Y. Mishael, U.
586 Rabinovitz, B. Rubin, Handbook of Clay Science, 2006. doi:10.1016/S1572-
587 4352(05)01021-4.

588 [51] É.C. Gaucher, P. Blanc, F. Bardot, G. Braibant, S. Buschaert, C. Crouzet, A. Gautier,
589 J.P. Girard, E. Jacquot, A. Lassin, G. Negrel, C. Tournassat, A. Vinsot, S. Altmann,
590 Modelling the porewater chemistry of the Callovian-Oxfordian formation at a regional
591 scale, Comptes Rendus - Geosci. 338 (2006) 917–930. doi:10.1016/j.crte.2006.06.002.

592

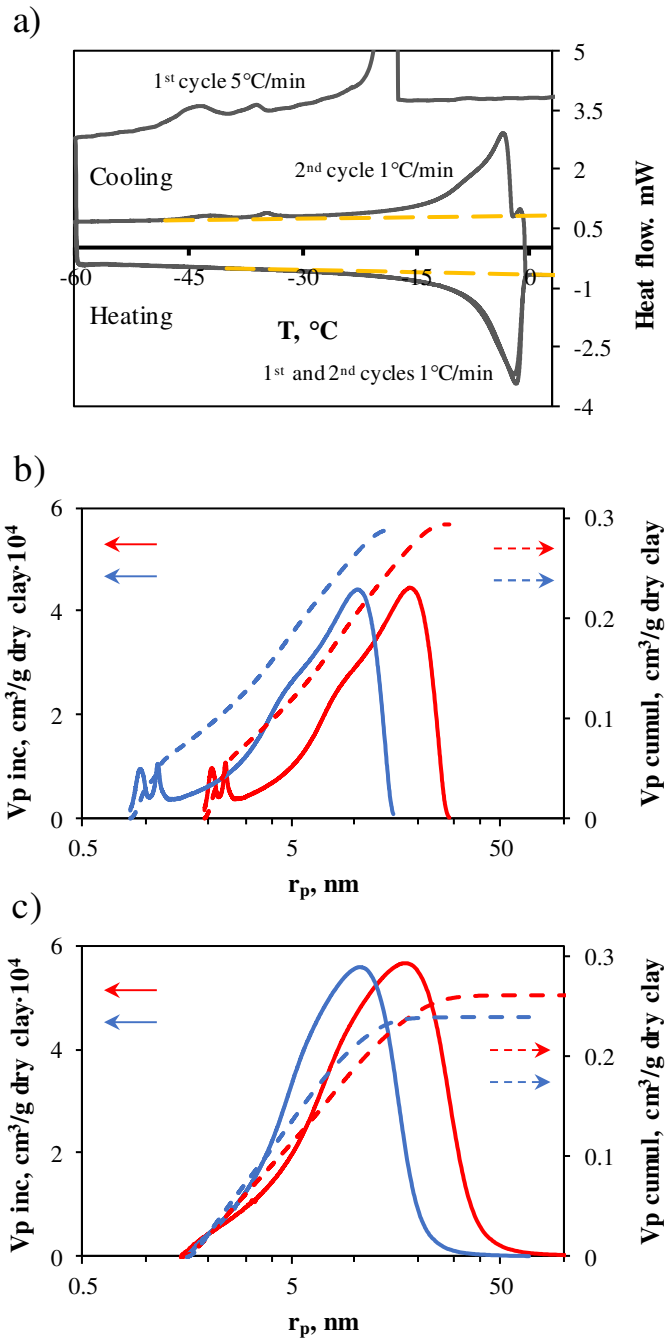

Figure 1. a) DSC curve of humidity-saturated Na-exchanged montmorillonite including 2 cycles of cooling and heating (grey line) together with the linear baseline (yellow discontinued line). Pore size distribution as determined from cooling (b) and heating (c) cycles of thermoporometry using the models of Brun considering cylindrical pore geometry (red trace) and Landry considering slit-type pore geometry (blue trace), solid and discontinued lines in b) and c) correspond to incremental and cumulative curves of pore size distribution. δ=0.6 nm and expression (7) accounting for ΔH_f variation with the temperature were used for pore volumes calculation.

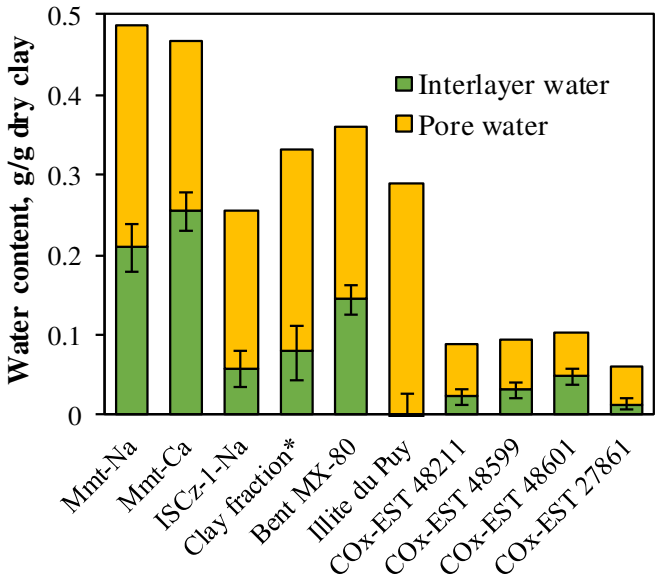

Figure 2. Water distribution determined from the results of thermoporometry (model of Brun considering cylindrical pore geometry, ΔH_f variation with the temperature described by expression (7), average between cooling and heating cycles, error bars are related to the thickness of a layer of non-freezing water: 0.3-0.9 nm) and thermogravimetric analysis for a series of clays. * - clay fraction extracted from COx-EST 51769 sample.

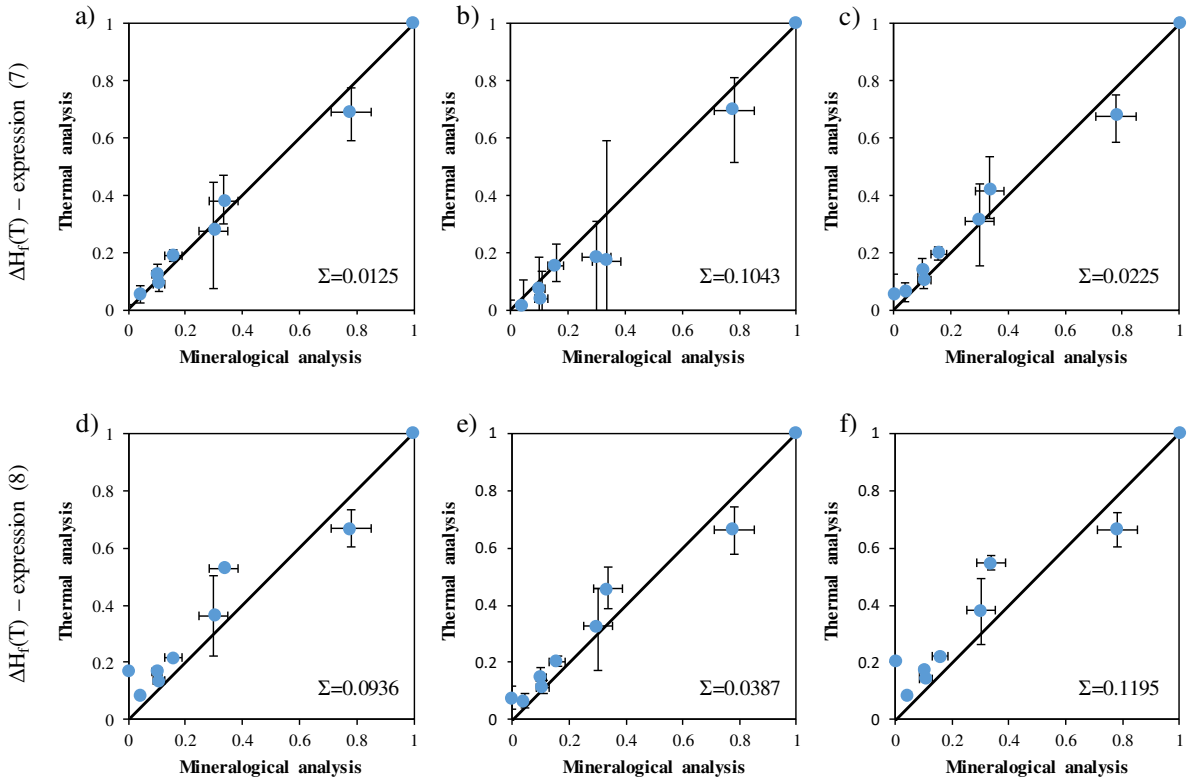

Figure 3. Comparison of smectite fraction for a series of clays, determined by mineralogical analysis and by thermogravimetric analysis combined with different approaches of thermoporometry: a) Model of Brun/cylindrical pore geometry/expression (7) for $\Delta H_f=f(T)$, b) Model of Landry/cylindrical pore geometry/expression (7) for $\Delta H_f=f(T)$, c) Model of Landry/slit pore geometry/expression (7) for $\Delta H_f=f(T)$, d) Model of Brun/cylindrical pore geometry/expression (8) for $\Delta H_f=f(T)$, e) Model of Landry/cylindrical pore geometry/expression (8) for $\Delta H_f=f(T)$, f) Model of Landry/slit pore geometry/expression (8) for $\Delta H_f=f(T)$. Σ - residual sum of squares between smectite fraction determined by thermal and by mineralogical analysis. Vertical error bars: difference between cooling and heating cycles, horizontal error bar: uncertainty of mineralogical composition.

Table 1. The maxima on pore size distribution curves for humidity-saturated clay systems as determined by thermoporometry (approaches of Brun and Landry).

Material	r_p model of Brun, nm		r_p model of Landry, nm	
	Cooling	Heating	Cooling	Heating
Model clay phases				
Mmt – Na	18.6 9.0 2.2	18.6	10.3 5.0 1.0	12.2
Mmt – Ca	11.8 7.3 2.4	10.4	6.6 4.2 1.2	7.2
ISCz-1 – Na	18 2.5	19	10	12
Illite du Puy – Na	7.3 12	11	4 5.6	7.9
Complex clay systems				
Bent MX-80 – Na	24.3 9.7 2.8	32	13.4 5 1.2	21
COx-EST 51769* – Na	18.8 2.4	15.8	10.5	10.4
COx-EST 48211	14-2	8.7	8-1	4.8
COx-EST 48599	10-2	8.5	5.5-1	5.9
COx-EST 48601	10.4-2	5.8	6-1	4
COx-EST 27861	13.8 (broad)-3	8.6	7.65 1.2	12.6

* states for purified clay fraction, Mmt – montmorillonite, Bent - bentonite.

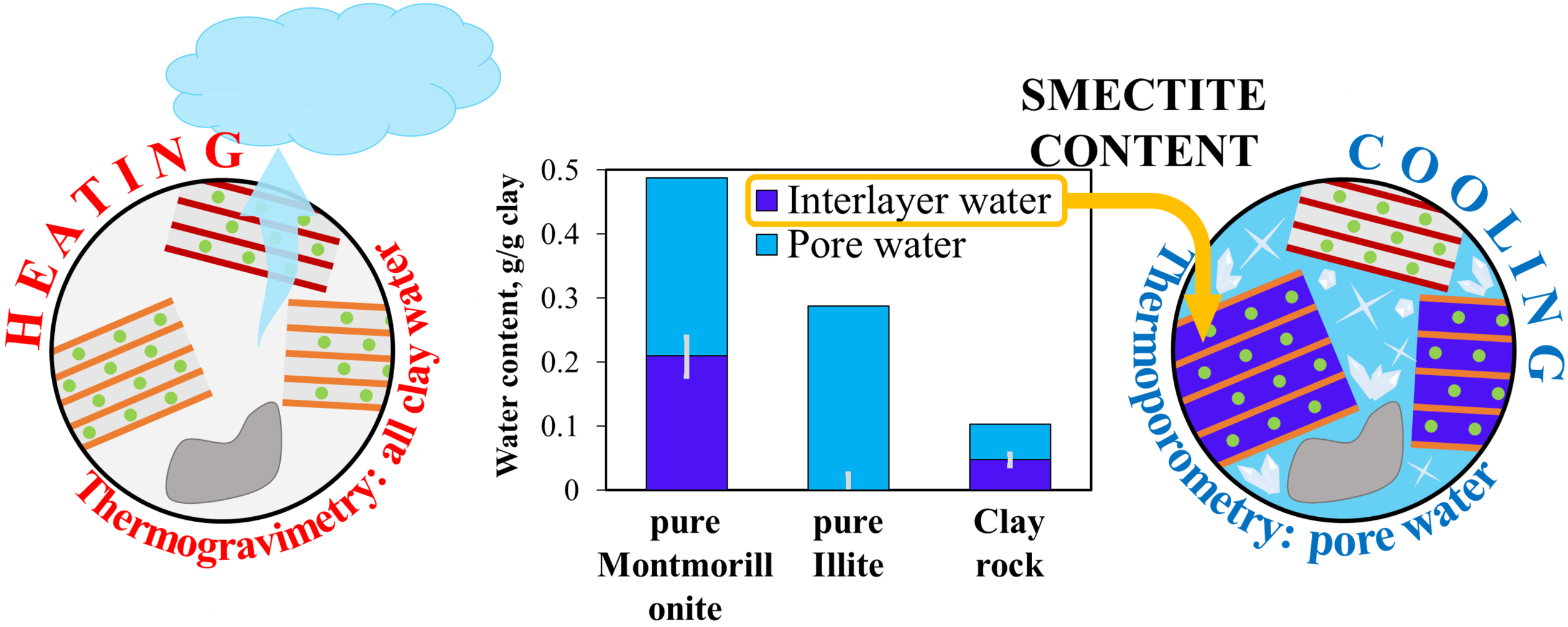
HEATING
Thermogravimetry: all clay water
SMECTITE CONTENT
Water content, g/g clay
0.5
0.4
0.3
0.2
0.1
0
Interlayer water
Pore water
pure Montmorillonite
pure Illite
Clay rock
COOLING
Thermoporometry: pore water